Supporting information

Synthesis and Surface Modification of Tin Nanoparticles and Their Electrochemical Performance in Lithium Ion Cells

Olga Riedel [ǂ,a], Anke Düttmann [ǂ,b], Simon Dühnen [a], Joanna Kolny-Olesiak [b], Christian Gutsche [b], Jürgen Parisi [b], Martin Winter [a,c], Martin Knipper [b,] and Tobias Placke [a,*]*

[a] University of Münster, MEET Battery Research Center, Institute of Physical Chemistry, Corrensstr. 46, 48149 Münster, Germany.

[b] Energy and Semiconductor Research Laboratory, Department of Physics, Carl von Ossietzky University of Oldenburg, 26129 Oldenburg, Germany.

[c] Helmholtz Institute Münster, IEK-12, Forschungszentrum Jülich GmbH, Corrensstr. 46, 48149 Münster, Germany.

[ǂ] authors contributed equally to this work.

<u>*Correspondence:</u>

tobias.placke@uni-muenster.de (T.P.), knipper@uni-oldenburg.de (M.K.)

Table S1. Initial weights of the different ligands and volume of the solvent formamide for the ligand exchange reaction for Sn_S-*X* (particle size ≈20 nm) and Sn_L-*X* (particle size ≈20-200 nm) nanoparticles (ligands *X*= OH^-, S^{x-}, PVP or MPA).

Sample	Mass of ligand / mg	Volume of formamide / mL
Sn_S-OH	400	400
Sn_L-OH	800	400
Sn_S-PVP	5000	400
Sn_L-PVP	4000	400
Sn_S-S	1560	600
Sn_L-S	1560	180
Sn_S-MPA	1060	600
Sn_L-MPA	1060	400

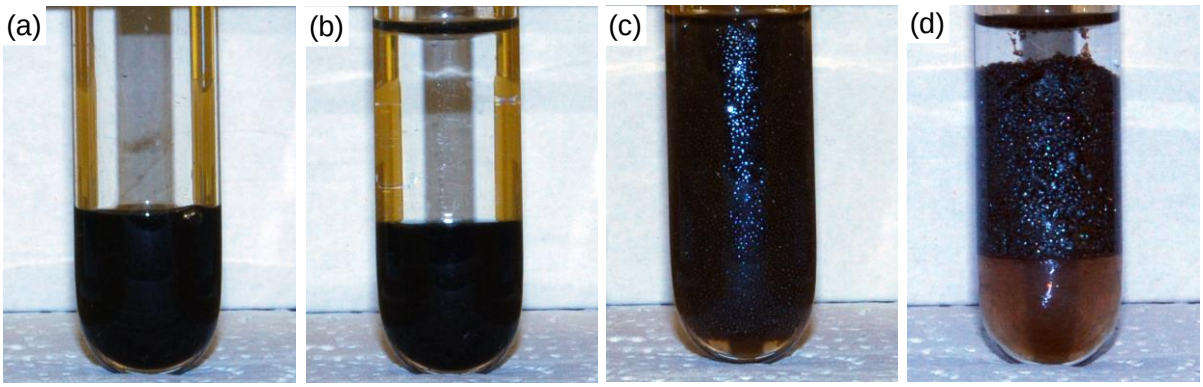

Figure S1. Photographs of the different steps during the ligand exchange starting with (a) the original oleic acid-capped nanoparticles in chloroform, (b) the adding of the ligand-formamide solution, (c) the mixture and (d) the hydroxide-capped Sn nanoparticles in formamide separated from the chloroform solution.

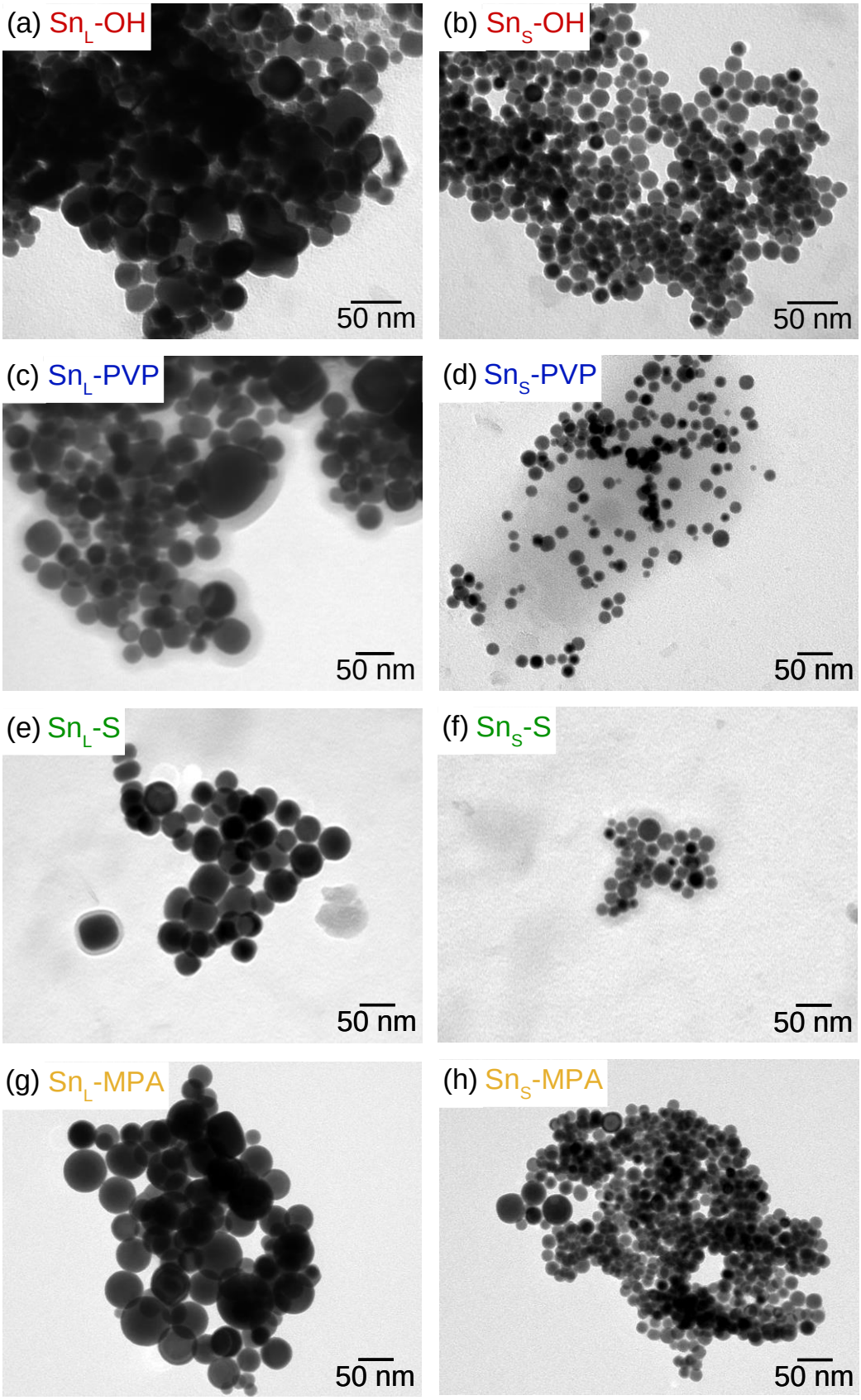

Figure S2. TEM images of Sn nanoparticles after the ligand exchange from oleic acid to (a) and (b) OH^-, (c) and (d) PVP, (e) and (f) S^{x-} and (g) and (h) MPA. The images on the left side ((a), (c), (e), (g)) belong to the Sn_L-*X* nanoparticles (particle size ≈20-200 nm) obtained from the precipitate and the images on the right side ((b), (d), (f), (h)) belong to the Sn_S-*X* nanoparticles (particle size ≈20 nm) from the centrifugate, respectively.

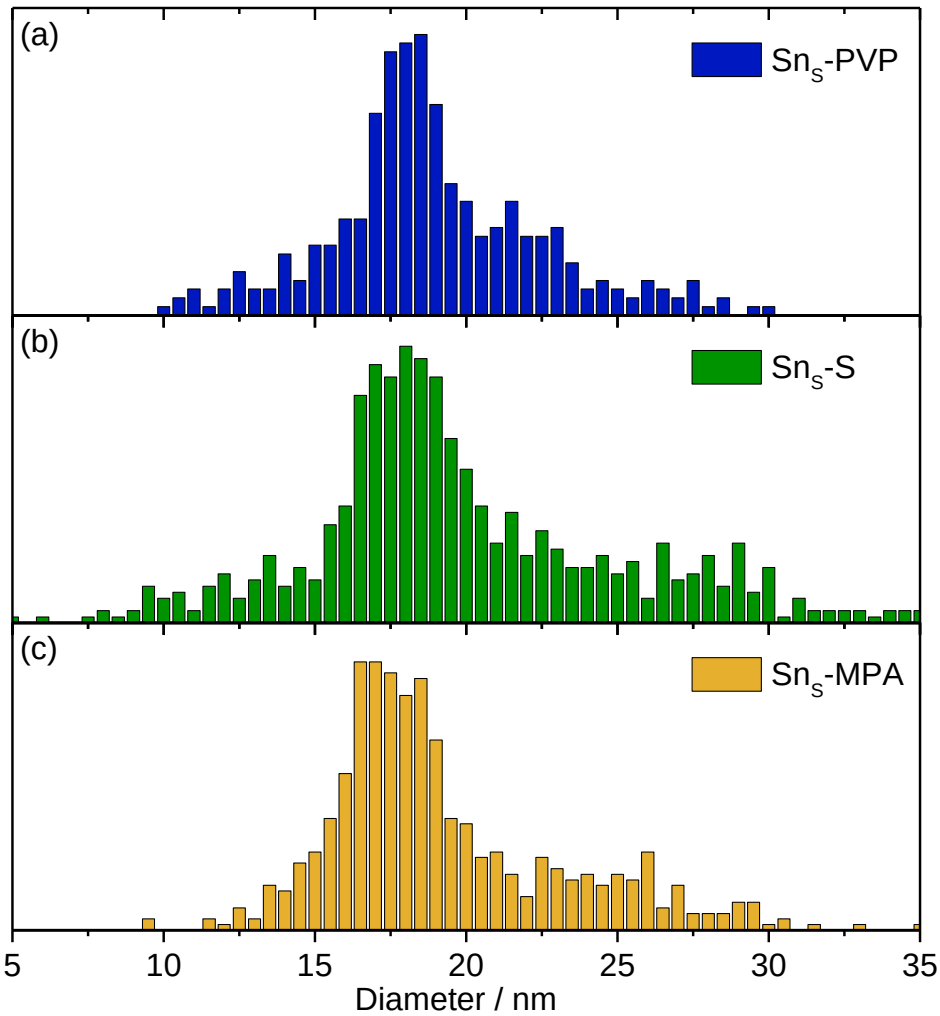

Figure S3. Particle size distributions of the synthesized oleic acid-capped Sn_S-*X* nanoparticles. *X*= (a) PVP, (b) S^{x-} and (c) MPA.

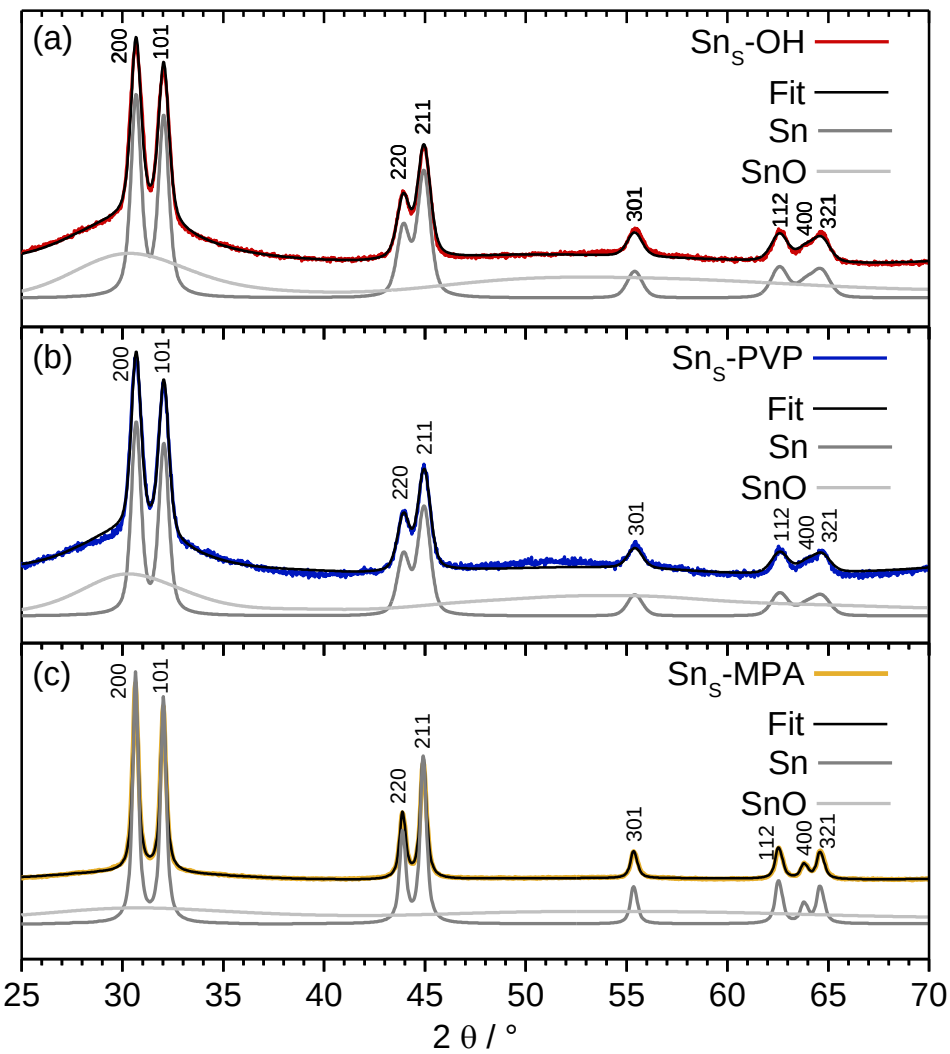

Figure S4. XRD patterns with Rietveld refinement of (a) OH^--capped, (b) PVP-capped and (c) MPA-capped Sn_S-*X* nanoparticles.

Table S2. Weight losses of Sn_S-*X* nanoparticles in a temperature range from 40-500 °C (according to **Figure 5**).

Sample	**Weight loss / %** **40-500 °C**
Sn_S-OH	12.9
Sn_S-PVP	47.5
Sn_S-S	3.8
Sn_S-MPA	34.3

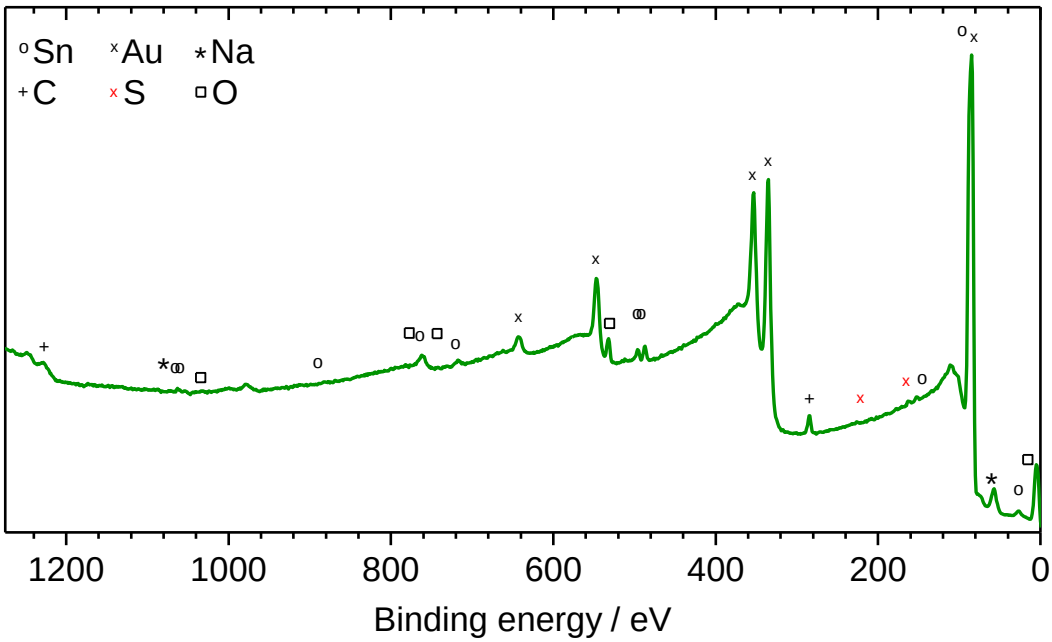

Figure S5. XPS survey spectrum of Sn_S-S. All rising signals are identified by the outlined elements.

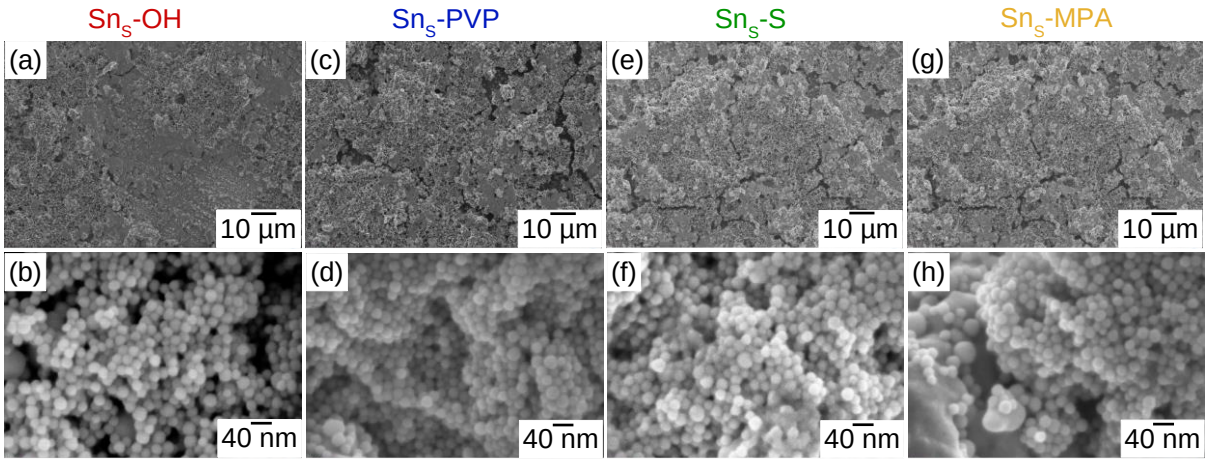

Figure S6. SEM images of surface-modified Sn_S-*X* nanoparticle composite electrodes (ligands *X*= OH^-, S^{x-}, PVP or MPA). (a), (c), (e) and (g) at 1kx magnification and (b), (d), (f) and (h) at 200kx magnification.

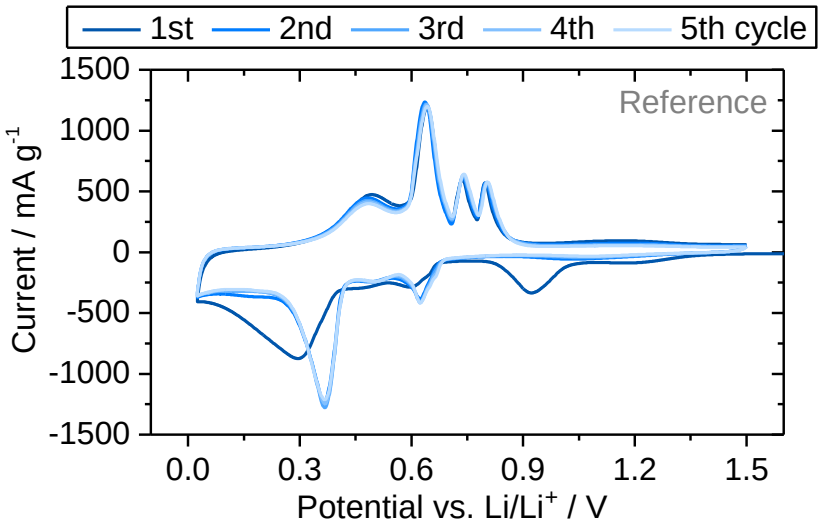

Figure S7. Cyclic voltammetry investigation of the reference Sn material (particle size: <150 nm). Measurement was conducted in Li metal (CE)‖Sn (WE) cells. Potential range (controlled *via* the RE): 0.025 to 1.5 V *vs*. Li/Li^+; scan rate: 0.1 mV s^{-1}.

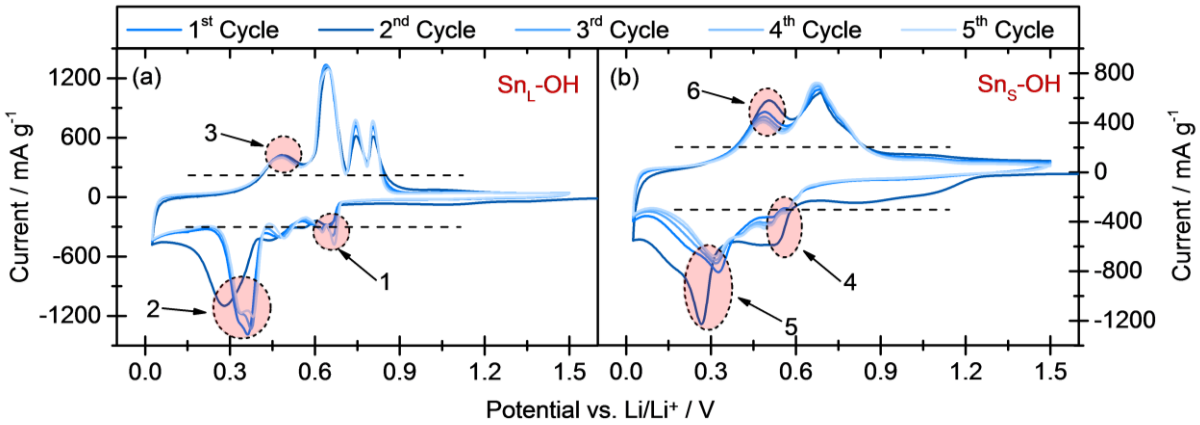

Figure S8. Cyclic voltammetry investigation of (a) Sn_L-OH and (b) Sn_L-OH samples showing the different lithiation and de-lithiation peaks (1-6), as summarized in **Table S3**. Measurement was conducted in Li metal (CE)‖Sn (WE) cells. Potential range (controlled *via* the RE): 0.025 to 1.5 V *vs*. Li/Li^+; scan rate: 0.1 mV s^{-1}.

Table S3. Overview of lithiation and de-lithiation peak potentials from cyclic voltammetry investigations of the different Sn_S-*X* and Sn_L-*X* samples (data are obtained from **Figure 7**). The corresponding peaks are exemplarily shown in **Figure S8** for the Sn_S-OH and Sn_L-OH samples.

Sample	**Cycle**	**Peak (1) Lithiation potential *vs.* Li/Li$^+$ / V**	**Peak (2) Lithiation potential *vs.* Li/Li$^+$ / V**	**Peak (3) De-lithiation potential *vs.* Li/Li$^+$ / V**
Sn_L-OH	1	0.644	0.284	0.483
	2	0.655	0.362	0.480
Sn_L-PVP	1	0.671	0.379	0.464
	2	0.667	0.344	0.465
Sn_L-S	1	0.674	0.378	0.466
	2	0.674	0.381	0.464
Sn_L-MPA	1	0.668	0.353	0.475
	2	0.670	0.341	0.478

Sample	**Cycle**	**Peak (4) Lithiation potential *vs.* Li/Li$^+$ / V**	**Peak (5) Lithiation potential *vs.* Li/Li$^+$ / V**	**Peak (6) De-lithiation potential *vs.* Li/Li$^+$ / V**
Sn_S-OH	1	0.533	0.267	0.504
	2	0.576	0.325	0.488
Sn_S-PVP	1	---	0.178	0.516
	2	---	0.226	0.501
Sn_S-S	1	0.685	0.297	0.507
	2	0.585	0.315	0.490
Sn_S-MPA	1	0.571	0.314	0.491
	2	0.639	0.329	0.469

Table S4. Overview of the specific discharge (=de-lithiation) capacity in selected cycles, capacity retention after the 100th cycle and the 1st cycle Coulombic efficiency of the different Sn_S-*X* and Sn_L-*X* samples during the long-term charge/discharge cycling investigations (according to **Figure 8**).

Active material	Specific discharge capacity / mAh g^{-1}			Capacity retention / %	Coulombic efficiency / %
	1st cycle	4th cycle	100th cycle	100th cycle	1st cycle
Sn_S-OH	930 ± 33	780 ± 4	739 ± 9	95 ± 1	44 ± 3
Sn_S-PVP	752 ± 10	642 ± 6	574 ± 12	61 ± 2	40 ± 1
Sn_S-S	784 ± 21	617 ± 17	623 ± 18	85 ± 2	43 ± 3
Sn_S-MPA	721 ± 35	651 ± 61	531 ± 3	72 ± 1	48 ± 4
Sn_L-OH	694 ± 24	660 ± 41	449 ± 23	64 ± 2	72 ± 3
Sn_L-PVP	792 ± 19	604 ± 9	361 ± 14	59 ± 2	70 ± 2
Sn_L-S	736 ± 28	486 ± 64	219 ± 41	46 ± 4	75 ± 3
Sn_L-MPA	759 ± 10	671 ± 45	321 ± 4	47 ± 3	72 ± 2
Reference	796 ± 2	742 ± 6	335 ± 4	42 ± 1	76 ± 3

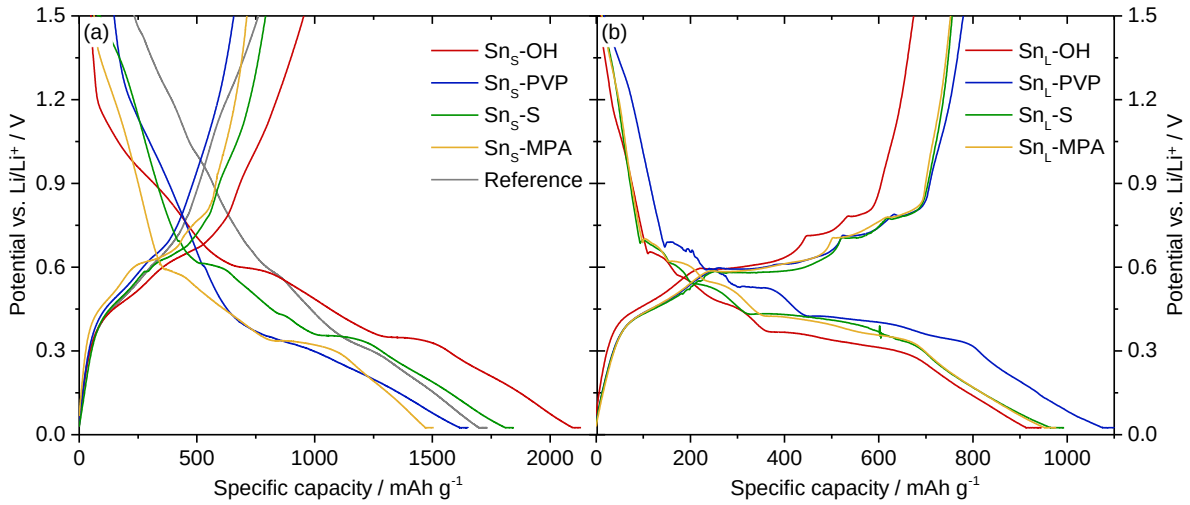

Figure S9. Electrode potential *vs*. specific capacity curves from the 1st cycle of constant current/constant potential charge/discharge cycling (at 0.1C) for (a) Sn_s-*X* nanoparticles and (b) Sn_L-*X* nanoparticles. All measurements were conducted in Li metal (CE)‖Sn (WE) cells. Potential range (controlled *via* the RE): 0.025 to 1.5 V *vs*. Li/Li$^+$. Data are obtained from results **Figure 8** (a) and (c) of the manuscript.

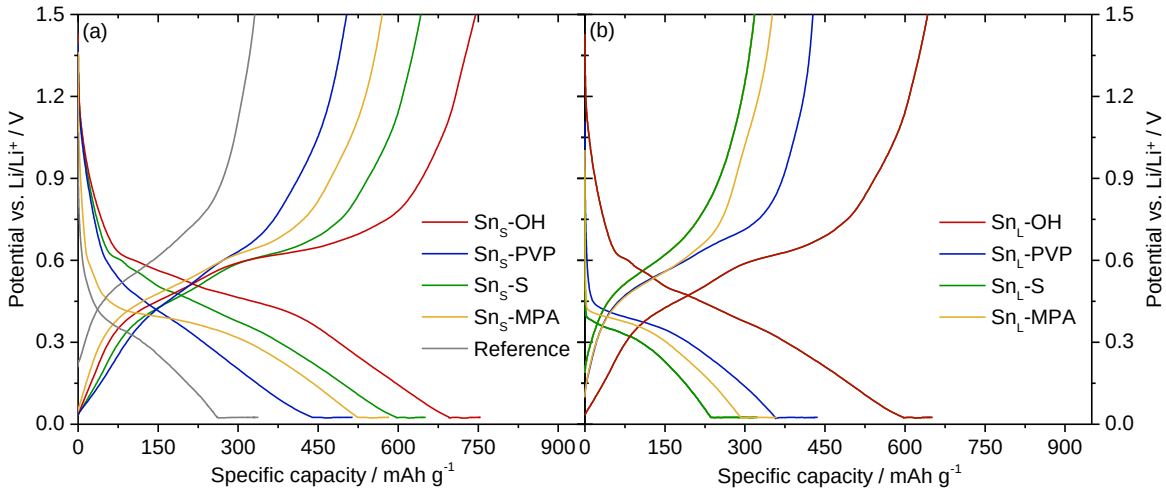

Figure S10. Electrode potential *vs*. specific capacity curves from the 100th cycle of constant current/constant potential charge/discharge cycling (at 1C) for (a) Sn_s-*X* nanoparticles and (b) Sn_L-*X* nanoparticles. All measurements were conducted in Li metal (CE)‖Sn (WE) cells. Potential range (controlled *via* the RE): 0.025 to 1.5 V *vs*. Li/Li$^+$. Data are obtained from results **Figure 8** (a) and (c) of the manuscript.

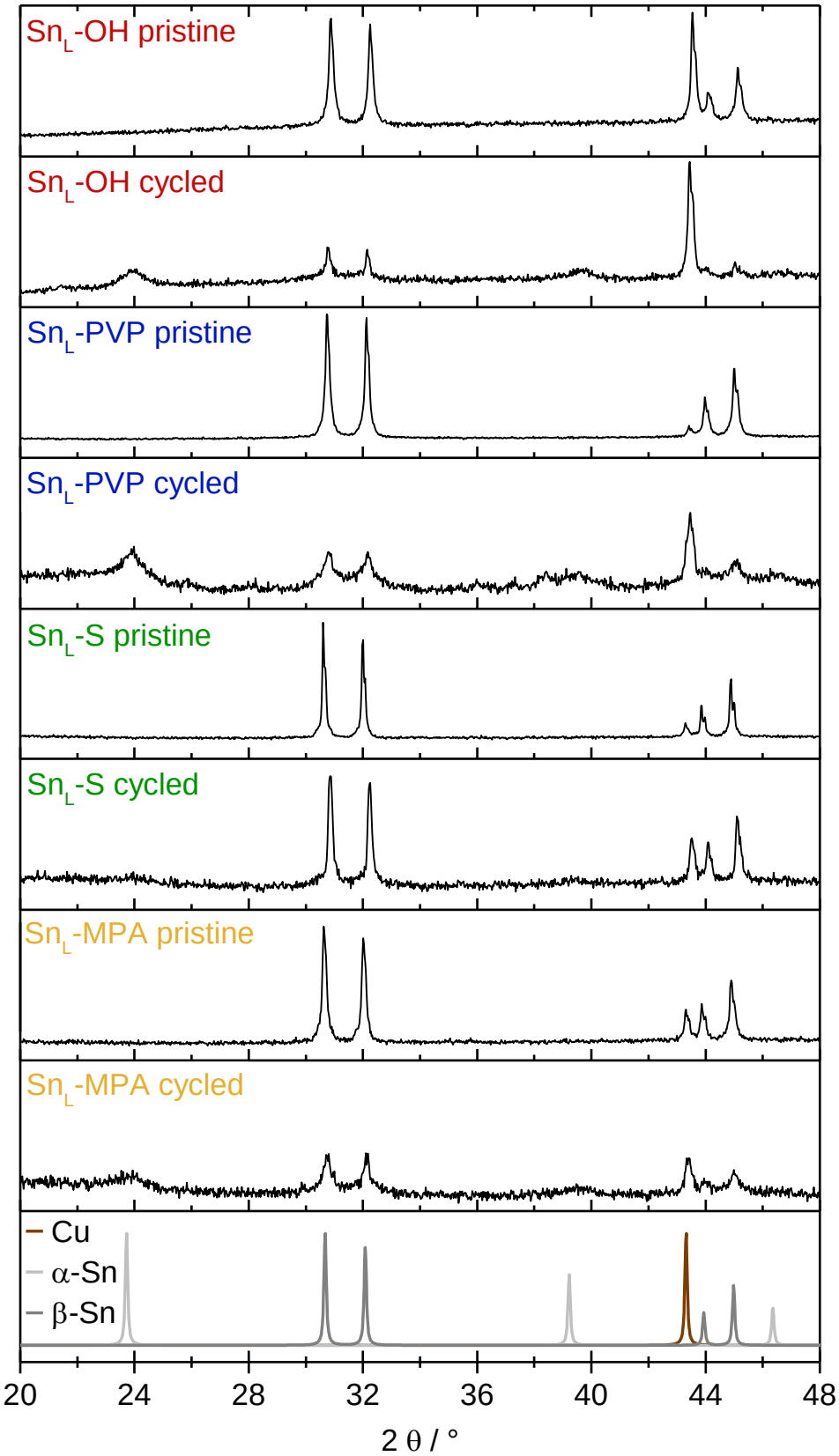

Figure S11. X-ray diffraction patterns of pristine and cycled Sn_L-*X* nanoparticle composite electrodes. All cycled electrodes show additional α-Sn reflections.

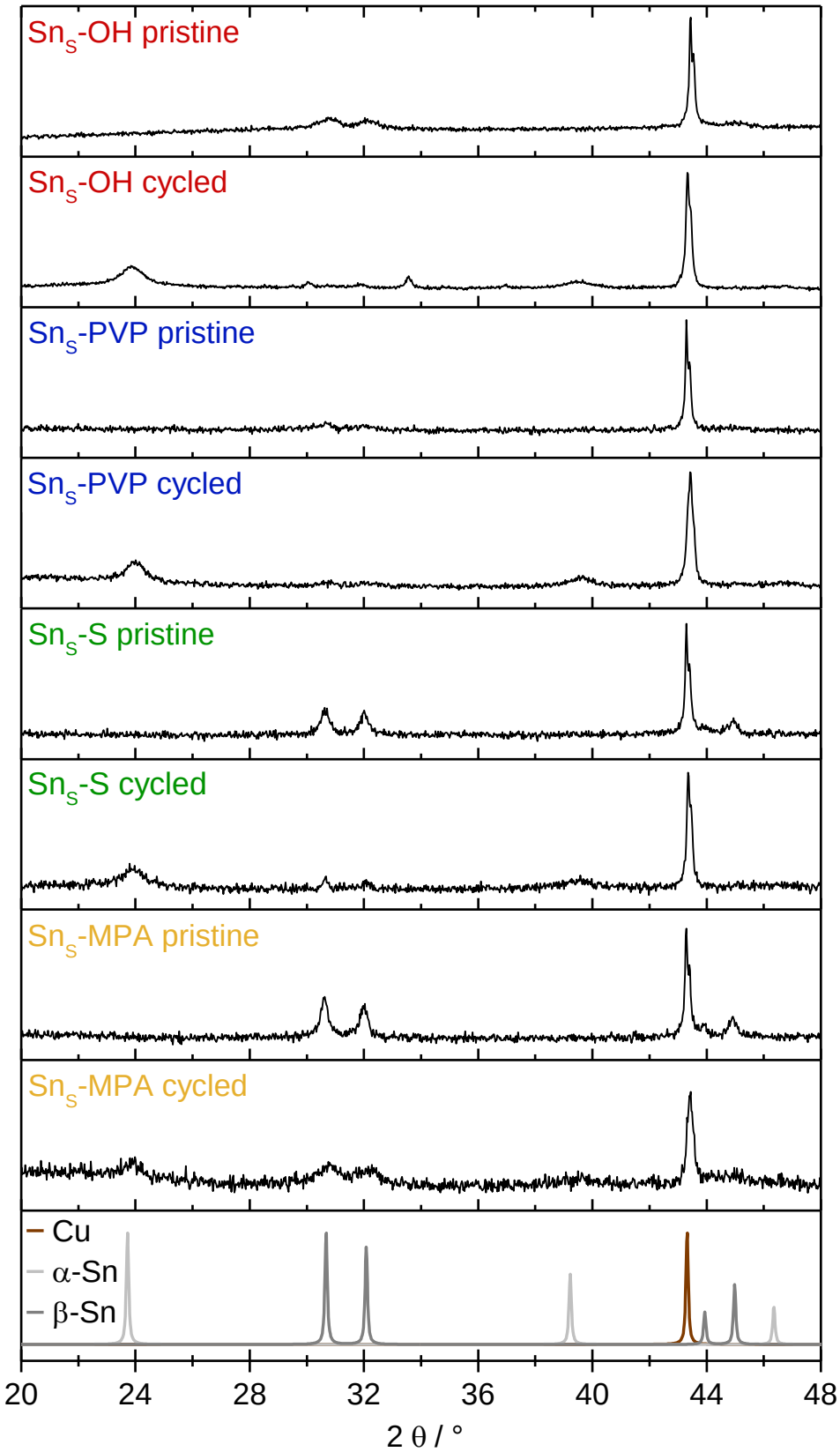

Figure S12. X-ray diffraction patterns of pristine and cycled Sns-*X* nanoparticle composite electrodes. All cycled electrodes show additional α-Sn reflections.

Table S5. Overview of electrochemical performance data of different tin-based anode materials for lithium ion batteries in comparison to the results of this work.

Sample	1st cycle specific discharge capacity / mAh g^{-1}	1st cycle Coulombic efficiency / %	100th cycle specific discharge capacity / mAh g^{-1}	Applied current during cycling / A g^{-1}	Electrode composition (Active mat.: cond. carbon: binder) / %	Electrolyte
Core/shell Sn_S-OH nanoparticles (this work)	930 ± 33	44 ± 3	739 ± 9	≈1.0	82 : 10 : 8	1 M $LiPF_6$ in EC:DEC 3:7 (by wt.), 2 wt.% VC, 2 wt.% FEC
Tin nanoparticles impregnated in nitrogen-doped graphene[1]	≈788	≈65	≈481	≈0.1	80 : 10 : 10	1 M $LiPF_6$ in EC:DMC:VC (1:1:0.04 by vol.)
Encapsulated Sn nanoparticles in amorphous carbon nanotubes[2]	≈900	≈63	≈749	≈0.2	70 : 20 : 10	1 M $LiPF_6$ in EC:DEC (1:1 by wt.)
Ultrafine Sn@C nanorods[3]	≈915	≈70	≈550	≈1.0	60 : 20 : 20	1 M $LiPF_6$ in EC:DEC:EMC (1:1:1 by vol.)
Inorganically capped Sn and Sn/SnO_2 nanocrystals[4]	≈1000	≤45	≈700	≈1.0	30 : 45 : 25	1 M $LiPF_6$ in EC:DMC 1:1 (by wt.), 3 wt.% FEC
Nanostructured Sn–C composite[5]	≈450	≤40	≈450	≈0.1	80 : 10 : 10	1 M $LiPF_6$ in EC:DMC 1:1 (by wt.)
Tin nanoparticle loaded graphite[6]	≈434	≈64	≤300 (after 60 cycles)	≈0.4 mA/cm^2	80 : 10 : 10	1 M $LiPF_6$ in EC:DMC 1:1 (by wt.)
Sn/SnO_x-loaded hollow carbon spheres on graphene nanosheets[7]	≈815	≈62	≈342	≈1.0	70 : 20 : 10	1.3 M $LiPF_6$ in EC:DEC 3:7 (by wt.), 10 wt.% FEC
Ultrasmall Sn nanoparticles embedded in spherical hollow carbon[8]	≈743	≈72	≈423	≈4.0	80 : 10 : 10	1 M $LiPF_6$ in EC:DMC 1:1 (by vol.)

Carbon-wrapped core–shell nanospheres of tin-graphitized carbon[9]	≈900	<80	≈450	≈1.0	80 : 10 : 10	1 M $LiPF_6$ in EC:DMC 1:1 (by vol.)
Nano-Sn/hard carbon composite[10]	≈440	≈76	≈300 (after 23 cycles)	≈0.1 mA/cm^2	90 : 5 : 5	1 M $LiPF_6$ in EC:DMC 1:1 (by vol.)
Ultrasmall Sn nanoparticles embedded in nitrogen-doped porous carbon[11]	≈1000	≈75	≈1000	≈0.2	80 : 10 : 10	1 M $LiPF_6$ in EC:DEC 1:1 (by vol.)

Wang *et al.*[6] and Zhang *et al.*[12] reported further electrochemical data of various Sn/graphite and SnO_2/graphite negative electrode materials for lithium ion batteries. Kamali and Frey[13] also reported performance data of different Sn-based anode materials.

References

(1) Zhou, X.; Bao, J.; Dai, Z.; Guo, Y.-G. Tin Nanoparticles Impregnated in Nitrogen-Doped Graphene for Lithium-Ion Battery Anodes. *The Journal of Physical Chemistry C* **2013,** *117* (48), 25367-25373, DOI: 10.1021/jp409668m.

(2) Zhou, X.; Yu, L.; Yu, X.-Y.; Lou, X. W. Encapsulating Sn Nanoparticles in Amorphous Carbon Nanotubes for Enhanced Lithium Storage Properties. *Adv. Energy Mater.* **2016,** *6* (22), 1601177, DOI: 10.1002/aenm.201601177.

(3) Ye, X.; Lin, Z.; Liang, S.; Huang, X.; Qiu, X.; Qiu, Y.; Liu, X.; Xie, D.; Deng, H.; Xiong, X.; Lin, Z. Upcycling of Electroplating Sludge into Ultrafine Sn@C Nanorods with Highly Stable Lithium Storage Performance. *Nano Lett.* **2019,** *19* (3), 1860-1866, DOI: 10.1021/acs.nanolett.8b04944.

(4) Kravchyk, K.; Protesescu, L.; Bodnarchuk, M. I.; Krumeich, F.; Yarema, M.; Walter, M.; Guntlin, C.; Kovalenko, M. V. Monodisperse and Inorganically Capped Sn and Sn/SnO_2 Nanocrystals for High-Performance Li-Ion Battery Anodes. *Journal of the American Chemical Society* **2013,** *135* (11), 4199-4202, DOI: 10.1021/ja312604r.

(5) Hassoun, J.; Derrien, G.; Panero, S.; Scrosati, B. A nanostructured Sn-C composite lithium battery electrode with unique stability and high electrochemical performance. *Advanced Materials* **2008,** *20* (16), 3169-3175, DOI: 10.1002/adma.200702928.

(6) Wang, Y.; Lee, J. Y.; Deivaraj, T. C. Tin Nanoparticle Loaded Graphite Anodes for Li-Ion Battery Applications. *Journal of The Electrochemical Society* **2004,** *151* (11), A1804-A1809, DOI: 10.1149/1.1799491.

(7) Lee, J.; Hwang, T.; Oh, J.; Kim, J. M.; Jeon, Y.; Piao, Y. Sn/SnO_x-loaded uniform-sized hollow carbon spheres on graphene nanosheets as an anode for lithium-ion batteries. *Journal of Alloys and Compounds* **2018,** *736*, 42-50, DOI: 10.1016/j.jallcom.2017.11.127.

(8) Zhang, N.; Wang, Y.; Jia, M.; Liu, Y.; Xu, J.; Jiao, L.; Cheng, F. Ultrasmall Sn nanoparticles embedded in spherical hollow carbon for enhanced lithium storage properties. *Chemical Communications* **2018,** *54* (10), 1205-1208, DOI: 10.1039/C7CC09095A.

(9) Mandi, Z.; Shihua, Q. Carbon-wrapped core–shell nanospheres of tin-graphitized carbon for superior lithium-ion battery. *Materials Letters* **2016,** *171*, 18-22, DOI: 10.1016/j.matlet.2016.02.015.

(10) Guo, B.; Shu, J.; Tang, K.; Bai, Y.; Wang, Z.; Chen, L. Nano-Sn/hard carbon composite anode material with high-initial coulombic efficiency. *Journal of Power Sources* **2008,** *177* (1), 205-210, DOI: 10.1016/j.jpowsour.2007.11.003.

(11) Zhu, Z.; Wang, S.; Du, J.; Jin, Q.; Zhang, T.; Cheng, F.; Chen, J. Ultrasmall Sn Nanoparticles Embedded in Nitrogen-Doped Porous Carbon As High-Performance Anode for Lithium-Ion Batteries. *Nano Lett.* **2014,** *14* (1), 153-157, DOI: 10.1021/nl403631h.

(12) Zhang, M.; Wang, T.; Cao, G. Promises and challenges of tin-based compounds as anode materials for lithium-ion batteries. *International Materials Reviews* **2015,** *60* (6), 330-352, DOI: 10.1179/1743280415Y.0000000004.

(13) Kamali, A. R.; Fray, D. J. Tin-Based Materials as Advanced Anode Materials for Lithium Ion Batteries: A Review. *Reviews on Advanced Materials Science* **2011,** *27* (1), 14-24.